

# Charge radii and structural evolution in Sr, Zr, and Mo isotopes

R. Rodríguez-Guzmán<sup>a</sup>, P. Sarriguren<sup>a</sup>, L.M. Robledo<sup>b</sup>, S. Perez-Martin<sup>b,1</sup>

<sup>a</sup>*Instituto de Estructura de la Materia, CSIC, Serrano 123, E-28006 Madrid, Spain*

<sup>b</sup>*Departamento de Física Teórica, Módulo 15, Universidad Autónoma de Madrid, 28049-Madrid, Spain.*

---

## Abstract

The evolution of the ground-state nuclear shapes in neutron-rich Sr, Zr, and Mo isotopes, including both even-even and odd- $A$  nuclei, is studied within a self-consistent mean-field approximation based on the D1S Gogny interaction. Neutron separation energies and charge radii are calculated and compared with available data. A correlation between a shape transition and a discontinuity in those observables is found microscopically. While in Sr and Zr isotopes the steep behavior observed in the isotopic dependence of the charge radii is a consequence of a sharp prolate-oblate transition, the smooth behavior found in Mo isotopes has its origin in an emergent region of triaxiality.

*Keywords:*

*PACS:* 21.60.Jz, 21.10.Ft, 27.60.+j

---

## 1. Introduction

The study of the properties of unstable nuclei both theoretically and experimentally is nowadays one of the most active and fruitful research lines in nuclear physics. Nuclear systems with very unusual  $N/Z$  ratios are proper candidates to get insight into the nuclear interaction and the impact that the associated dynamics might have in low-energy observables like the ground-state deformation and derived quantities like moments of inertia or vibrational excitation energies [1]. The understanding of the properties of those nuclei also has important consequences in the understanding of other physical processes like stellar nucleosynthesis of heavy elements. In particular, the neutron-rich Sr, Zr, and Mo isotopes with mass numbers  $A = 100 - 110$  are of special interest for various reasons. One of them is the role that these isotopes play in the nucleosynthesis of heavy nuclides in the astrophysical  $r$  process. Their masses and decay properties are an essential input to model the path, the isotopic abundances and the time scale of the  $r$  process in a reliable way [2]. In addition, from the nuclear structure point of view, this region is characterized by a strong competition between various shapes, giving rise to shape instabilities that lead to coexisting nuclear shapes, as well as to sudden shape transitions in isotopic chains [3].

It has been shown that the ground states of Sr, Zr and Mo isotopes with  $N$  ranging from the magic number  $N = 50$  up to  $N \sim 60$  are weakly deformed, but they undergo a shape transition from nearly spherical to well deformed prolate (or oblate) deformations as  $N = 60$  is approached and crossed. Evidence for such an abrupt shape change includes  $2^+$  lifetime measurements [4, 5] as well as quadrupole moments for rotational bands

[6]. Signatures of triaxiality in Mo isotopes from spectroscopic studies of high-spin states have also been identified [7]. Heavier Sr and Zr ( $A \sim 110$ ) isotopes display an axially symmetric well deformed shape. Above this region, it has been suggested that the  $N = 82$  shell closure might be quenched far from stability. This quenching has been predicted by different models [8], but still weak experimental evidence has been found.

Masses (nuclear binding energies) and charge radii are considered among the most sensitive observables to explore the structural evolution in nuclei far from the valley of stability, where other types of spectroscopic experiments are prohibitive because of the low production rates and short lifetimes of these unstable isotopes. Discontinuities in the systematics of particular mass regions suggest a change in the structure of the ground states among the configurations competing for the lowest energy. Drastic changes in the mean square (ms) radius of the charge distributions in regions of transitional nuclei may also be indicators of structural changes related to the nuclear deformation.

## 2. Theoretical framework

In this work we study this phenomenology in the framework of the self-consistent Hartree-Fock-Bogoliubov (HFB) approximation based on the finite range and density dependent Gogny interaction [9] with the parametrization D1S [10]. The HFB wave functions are expanded in a harmonic oscillator basis containing enough number of shells to achieve convergence of the results for all the nuclei studied.

The quadrupole deformations at equilibrium are obtained self-consistently by a minimization procedure. Nevertheless, constrained calculations have also been performed to generate potential energy curves (PEC) or potential energy surfaces (PES) to study the evolution with the number of nucleons of

---

<sup>1</sup>Currently at CIEMAT Nuclear Fission Division, Av. Complutense 22, Edif. 17, 28040 Madrid (SPAIN)

the various shapes associated to the different minima displayed by the PECs or PESs. This has been accomplished preserving axial symmetry first, and allowing afterward for triaxiality in the most relevant isotopes where shape transitions take place. Hence, we have constrained the mean value of the quadrupole operators  $\hat{Q}_{20}$  and  $\hat{Q}_{22}$  (in the axial case only the former is constrained),

$$Q_{20} = \frac{1}{2} \langle \Phi_{\text{HFB}} | 2z^2 - x^2 - y^2 | \Phi_{\text{HFB}} \rangle, \quad (1)$$

$$Q_{22} = \frac{\sqrt{3}}{2} \langle \Phi_{\text{HFB}} | x^2 - y^2 | \Phi_{\text{HFB}} \rangle. \quad (2)$$

In the triaxial figures we plot  $Q - \gamma$  planes, where

$$Q = \sqrt{Q_{20}^2 + Q_{22}^2} \quad (3)$$

and  $\gamma$  is the angle defined as  $\tan \gamma = Q_{22}/Q_{20}$  [11]. With this definition an axially symmetric prolate mass distribution has  $\gamma = 0^\circ$ , whereas the corresponding oblate one has  $\gamma = 60^\circ$ . The quadrupole deformation parameter  $\beta$  is defined in terms of the mass quadrupole moment  $Q_{20}$  and ms radius  $\langle r^2 \rangle$ ,

$$\beta = \sqrt{\frac{\pi}{5}} \frac{Q_{20}}{A \langle r^2 \rangle}. \quad (4)$$

For the description of odd- $A$  nuclei, we have extended the HFB formalism using blocking techniques. The blocked HFB wave function of the odd- $A$  system is in general given by

$$|\Phi_{\text{HFB}}\rangle_\alpha = \beta_\alpha^+ |\Phi_{\text{HFB}}\rangle, \quad (5)$$

where  $|\Phi_{\text{HFB}}\rangle$  is a reference even-even HFB vacuum ( $\beta_\alpha |\Phi_{\text{HFB}}\rangle = 0$ ) and  $\beta_\alpha^+$  is a quasiparticle creation operator. The index  $\alpha$  stands for the quasiparticle quantum numbers characterizing the blocked state (angular momentum projection  $K$  and parity in the case of axial symmetry). The ground state of the odd nucleus is determined by finding the blocked state that minimizes the total energy. In the present study we use the equal filling approximation (EFA), a prescription widely used in mean-field calculations to treat the dynamics of odd nuclei in a time-reversal invariant way. In this approximation the unpaired nucleon is treated in an equal footing with its time-reversed state by sitting half a nucleon in a given orbital and the other half in the time-reversed partner. This procedure has been recently justified microscopically, showing that the EFA can be described in terms of a mixed state density operator and the equations to be solved are a direct consequence of the variational principle over the energy of such mixed state [12]. It has also been shown that the EFA and the exact blocking procedure are both strictly equivalent when the time-odd fields of the energy density functional are neglected [13]. Thus, EFA is sufficiently precise for most practical applications.

In this work, we present results for one-neutron ( $S_n$ ) and two-neutron ( $S_{2n}$ ) separation energies, which can be easily calculated from the binding energies  $BE$ ,

$$\begin{aligned} S_n(Z, N) &= -BE(Z, N) + BE(Z, N-1), \\ S_{2n}(Z, N) &= -BE(Z, N) + BE(Z, N-2). \end{aligned} \quad (6)$$

Charge radii and their differences are crucial quantities to study the systematics of the nuclear-shape changes as they can be measured with remarkable precision using laser spectroscopic techniques. They are obtained theoretically by folding the proton distribution of the nucleus with the finite size of the protons and the neutrons. The ms radius of the charge distribution in a nucleus can be expressed as

$$\langle r_c^2 \rangle = \langle r_p^2 \rangle_Z + \langle r_c^2 \rangle_p + (N/Z) \langle r_c^2 \rangle_n + r_{CM}^2, \quad (7)$$

where  $\langle r_p^2 \rangle_Z$  is the ms radius of the point proton distribution in the nucleus

$$\langle r_p^2 \rangle_Z = \frac{\int r^2 \rho_p(\vec{r}) d\vec{r}}{\int \rho_p(\vec{r}) d\vec{r}}, \quad (8)$$

$\langle r_c^2 \rangle_p = 0.80 \text{ fm}^2$  and  $\langle r_c^2 \rangle_n = -0.12 \text{ fm}^2$  are the ms radii of the charge distributions in a proton and a neutron, respectively.  $r_{CM}^2$  is a small correction due to the center of mass motion, which is evaluated according to Ref. [14]. It is worth noticing that the most important correction to the point proton ms nuclear radius, coming from the proton charge distribution  $\langle r_c^2 \rangle_p$ , vanishes when isotopic differences are considered, since it does not involve any dependence on  $N$ .

The variations of the charge radii in isotopic chains are related to deformation effects. Other structure effects like pairing or spin-orbit couplings have been considered [15, 16], but in this work they are fixed by the Gogny interaction. For an axially symmetric static quadrupole deformation  $\beta$  the increase of the charge radius with respect to the spherical value is given to first order by

$$\langle r^2 \rangle = \langle r^2 \rangle_{\text{sph}} \left( 1 + \frac{5}{4\pi} \beta^2 \right), \quad (9)$$

where usually  $\langle r^2 \rangle_{\text{sph}}$  is taken from the droplet model. Then, the measured radii have been used to estimate the changes in quadrupole deformation [17]. On the contrary, in this work we analyze the effect of the quadrupole deformation on the charge radii from a microscopic self-consistent approach.

### 3. Results

The PECs of the neutron-rich isotopes of Sr, Zr, and Mo from  $N = 50$  to  $N = 68$  have been calculated with the Gogny-D1S interaction. Our results fully agree with those of Ref. [18] that were obtained in the same framework. The main features of the shape evolution in the axial case can be summarized as follows: The isotopes with  $N = 50 - 54$  show a sharp PEC around the spherical minimum that becomes rather shallow at  $N = 56 - 58$ . Isotopes with  $N = 60$  are already deformed with oblate and prolate minima very close in energy. In the case of Sr isotopes the ground state is prolate, for Zr isotopes both oblate and prolate minima are found at about the same energy, while for Mo isotopes the ground state is oblate. Beyond  $N = 60$  the shapes become stable and for heavier isotopes we obtain basically similar results to  $N = 60$ . It is also worth mentioning the incipient emergence of a spherical solution in the heavier isotopes.

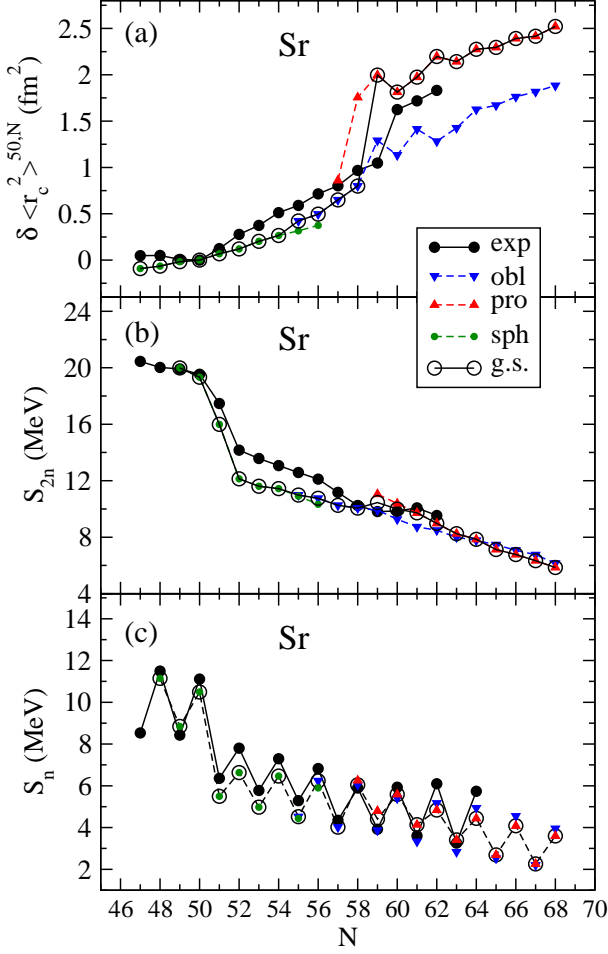


Figure 1: Calculated  $\delta \langle r_c^2 \rangle$  (a),  $S_{2n}$  (b), and  $S_n$  (c) in Sr isotopes compared to experimental data from Ref. [27] for masses and from Ref. [28] for radii. Results for prolate, oblate, and spherical minima are displayed with different symbols (see legend). Open circles correspond to ground-state results.

The shape change at  $N \sim 60$  has been predicted to a different extent by various theoretical models. Global calculations within the finite-range droplet model [19] with single-particle states obtained from folded Yukawa predict prolate quadrupole deformations increasing smoothly from  $N = 50$  up to  $N = 56$ , and then jumping suddenly to large deformations between  $N = 58$  and  $N = 60$ . At  $N = 62$  the shapes stabilize until a transition to oblate shapes is predicted at  $N = 74$  in Sr and Zr, and at  $N = 72$  in Mo. Triaxial calculations within this approach were carried out in Ref. [20], showing that only Mo isotopes have a tendency to triaxiality in this mass region.

The approach followed in Ref. [21], where PESs were studied within a finite-range liquid drop model modified by shell corrections taken from deformed Woods-Saxon potentials, suggests an oblate-prolate shape coexistence in Sr and Zr isotopes from  $N = 60 - 70$  with prolate ground states. Mo isotopes display in this case a soft behavior that develops triaxiality at  $N = 72, 74$ . Other calculations including rotational states in terms of the total Routhian surface, using non-axial Woods-Saxon potentials [22], predict two coexisting prolate and oblate minima for  $^{106-116}\text{Zr}$  isotopes, where the prolate ground state

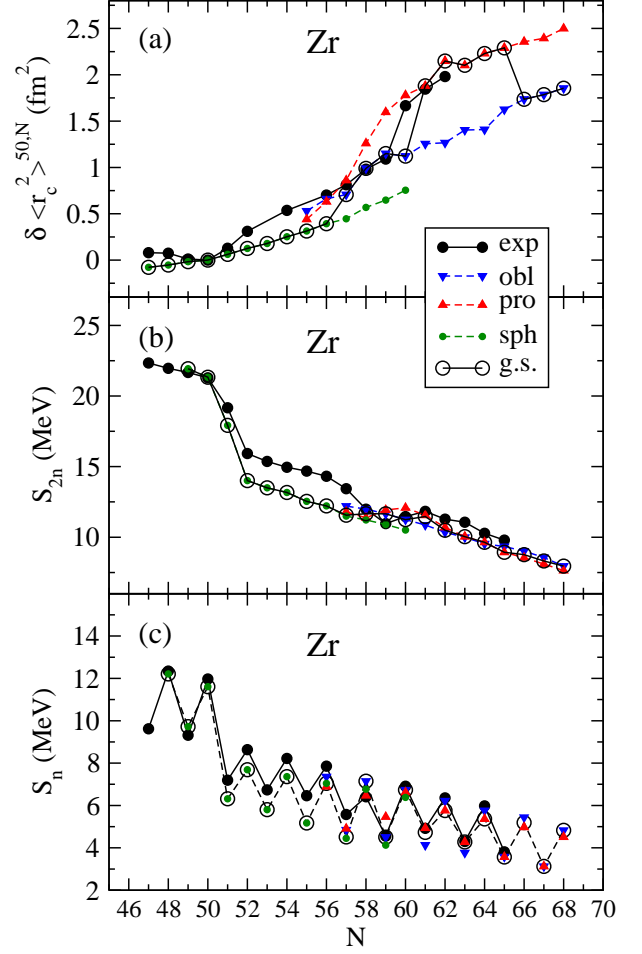


Figure 2: Same as in Fig. 1, but for Zr isotopes. Experimental data for masses and radii are from Refs. [27] and [29], respectively.

becomes oblate beyond  $^{110}\text{Zr}$ . The same calculations predict a  $\gamma$ -soft triaxial minimum for  $^{108}\text{Mo}$ .

Relativistic mean-field calculations [23] also show increasing prolate deformations from  $N = 50$  up to  $N = 60$ . In the region between  $N = 60$  and  $N = 70$  the deformations are stable for both Sr and Zr, whereas they change to oblate at  $N = 64$  in Mo. Triaxial PESs calculated from Skyrme HF+BCS were already published in Ref. [24], where the shape evolution along Kr, Sr, Zr, and Mo isotopes was studied. Finally, large scale studies of quadrupole correlation energies and ms charge radii, based on both Skyrme-SLy4 [25] and Gogny-D1S [26] effective interactions have been carried out recently. In summary, most of the theoretical nuclear models predict increasing deformations up to  $N = 60$ , where oblate and prolate shapes are developed and exhibit minima at close energies. Which of them becomes the ground state depends on subtle details of the calculation. At variance with the calculations mentioned above, in the present work we also consider odd-A nuclei in the framework of the EFA.

In the next figures we can see the results obtained for  $\delta \langle r_c^2 \rangle^{50,N} = \langle r_c^2 \rangle^N - \langle r_c^2 \rangle^{50}$  in (a), for  $S_{2n}$  energies in (b), and for  $S_n$  energies in (c). Fig. 1 corresponds to Sr, Fig. 2 to

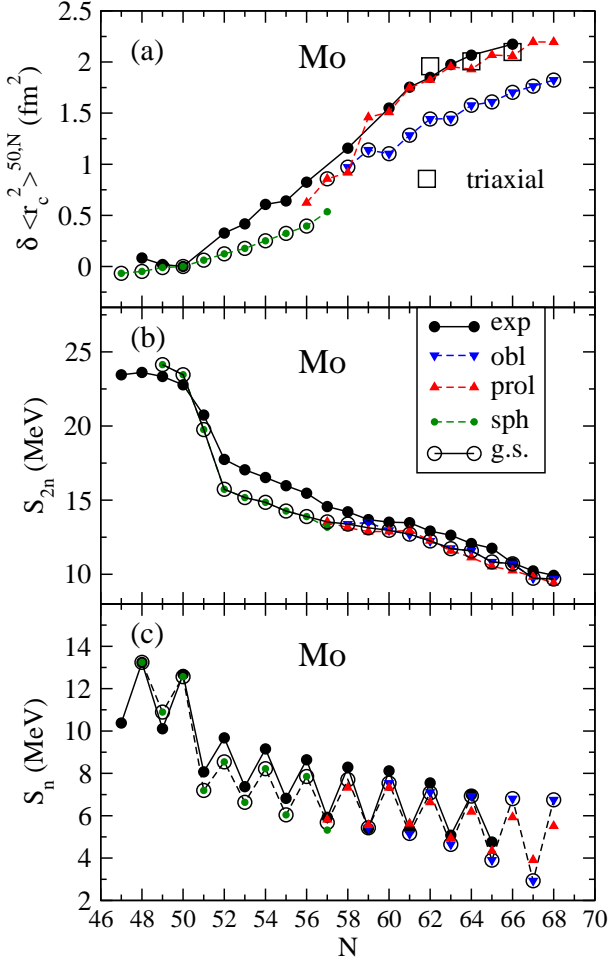


Figure 3: Same as in Fig. 1, but for Mo isotopes. Experimental data for masses and radii are from Refs. [27] and [17], respectively.

Zr, and Fig. 3 to Mo isotopes. In the three figures, results are shown as a function of the neutron number for all possible values of  $N$ , even or odd, in the range of interest. Experimental data have been taken from the mass measurements [27] and from laser spectroscopy experiments carried out at ISOLDE/CERN and at the IGISOL facility of the University of Jyväskylä [17, 28, 29]. Focusing on the experimental data, a consistent picture emerges. Besides the abrupt decrease of  $S_{2n}$  and  $S_n$  at  $N = 50$  corresponding to the shell closure, the evolution of the  $S_{2n}$  and  $S_n$  along the isotopic chains shows a change in the tendency around  $N = 60$  in Sr and Zr isotopes. This suggests a change in the ground-state shape of these isotopes. On the other hand, the chain of Mo isotopes shows a smoother behavior. These observations are confirmed by laser spectroscopy experiments measuring the nuclear ms radius. In this case, the shape change in Sr and Zr is observed in the form of a sudden increase of the ms charge radii at  $N = 58 - 60$ . Again, the Mo isotopic chain [17] displays a smooth behavior as the neutron number increases.

In these figures we also see the calculated values using the oblate (down triangles), prolate (up triangles) and spherical (dots) shapes corresponding to the local minima in the PECs.

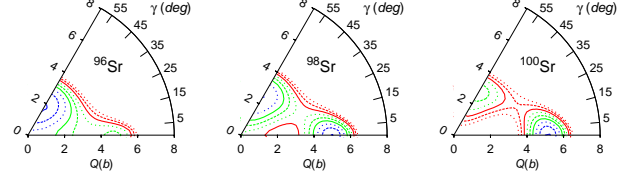


Figure 4:  $Q - \gamma$  planes for  $^{96,98,100}\text{Sr}$  isotopes with the Gogny-D1S interaction. The contour lines extend from the minimum up to 2 MeV higher in steps of 0.25 MeV.

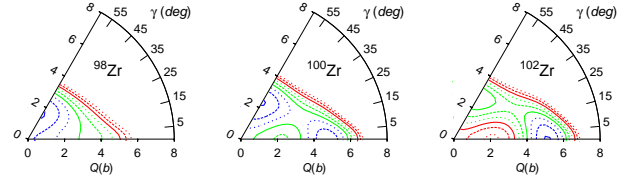


Figure 5: Same as in Fig. 4, but for  $^{98,100,102}\text{Zr}$  isotopes.

We also plot by open circles the theoretical values that correspond to the ground states of the corresponding isotopes. In general, the measured  $S_{2n}$  are reproduced reasonably well. The calculated shell gap at  $N = 50$  is larger than observed, but this is a well known feature related to any mean-field calculation. The discrepancy can be reduced considering dynamical correlations beyond mean field [25, 26]. Between  $N = 52$  and  $N = 58$ , the  $S_{2n}$  energies are underestimated by the calculations, while they are much better reproduced beyond  $N = 60$ . In our calculations a change in the tendency is observed at  $N \sim 60$ , which is more pronounced in Sr and Zr isotopes and almost disappears in Mo isotopes. However, the shoulder is less apparent than the experimental one due to the underestimation of the data below  $N = 60$ . Notice that the open circles at  $N = 59$  in  $S_{2n}$  and  $S_n$  do not coincide with any specific deformation (oblate or prolate) because they correspond to the difference between the prolate  $N = 59$  and the oblate  $N = 58$  in  $S_n$  and  $N = 57$  in  $S_{2n}$ . In the case of  $S_n$  energies, the amplitude of the odd-even staggering in  $S_n$  is well reproduced by the calculations indicating the validity of our theoretical description of odd-A nuclei. In general, the agreement is fairly good below  $N = 50$ . Then, the calculations underestimate the measured  $S_n$  values between  $N = 50$  and  $N = 60$ , being the net effect a displacement to slightly lower energies. The agreement improves substantially for heavier isotopes.

The evolution of the nuclear charge radii can be seen in panels (a) of Figs. 1, 2 and 3, where the radius, relative to that of the  $N = 50$  isotope, is plotted as a function of neutron number. Results for both even-even and odd-A isotopes are included in the plot. It is worth pointing out the almost negligible odd-even staggering observed both in the theoretical predictions and the experimental data. In Fig. 1, for Sr isotopes, we can see that the calculations follow nicely the measurements. There is a smooth increase of  $\delta \langle r_c^2 \rangle$  up to  $N = 58$ , then a sudden jump occurs at  $N = 60$  and again the increase is smooth for heavier isotopes. The encircled symbols indicate the shapes corresponding to the ground states obtained in our calculations. We can see that the lighter isotopes are spherical, then they change

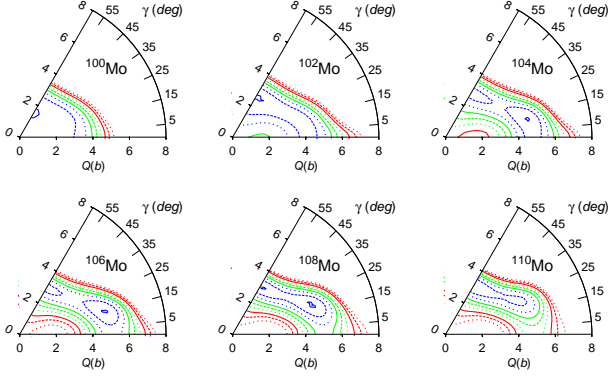


Figure 6: Same as in Fig. 4, but for  $^{100-110}\text{Mo}$  isotopes.

into oblate very smoothly and at about  $N = 60$  they become prolate. The observed jump corresponds to the transition from the oblate to the prolate shape since the oblate deformation is placed at  $\beta \sim -0.2$  while the prolate one appears with a different magnitude ( $\beta \sim 0.4$ ). Fig. 2(a) shows similar results for Zr isotopes. Here, the spherical shapes account for the behavior of  $\delta\langle r_c^2 \rangle$  up to  $N = 56$ . From  $N = 56$  up to  $N = 60$  there is a smooth transition to oblate shapes that become the ground states and reproduce quite well the experiment. Above  $N = 60$  we obtain prolate ground states with radii in agreement with the observed jump. For heavier isotopes (beyond  $N = 66$ ) we obtain again oblate shapes but there is no information in this region. Finally, Fig. 3(a) for Mo isotopes shows that the lightest isotopes are spherical changing into oblate shapes and increasing the  $\delta\langle r_c^2 \rangle$  very smoothly.

In general, we observe that the calculations from  $N = 54 - 60$  with spherical ground states underestimate the data for the nuclear radius in the three isotopic chains. One should notice that these spherical solutions are not very sharp but shallow minima as  $N$  increases. Thus, a possible explanation for the discrepancy in  $\delta\langle r_c^2 \rangle$  could be that configuration mixing plays an important role in these isotopes and the actual ground state will have contributions not only from the spherical configuration, but also from neighbor deformed states that will increase slightly the charge radii. In the case of Sr isotopes, the sudden change in  $\delta\langle r_c^2 \rangle$  occurs experimentally between  $N = 59$  and  $N = 60$ , whereas theoretically it appears between  $N = 58$  and  $N = 59$ . Similarly in Zr isotopes we obtain the change between  $N = 60 - 61$ , while experimentally is observed between  $N = 59 - 60$ . We do not think this discrepancy is significant since it is related to the subtle competition between prolate and oblate shapes. We should notice that in the isotopes where the shape is changing we get practically degenerate energies for oblate and prolate deformations and thus, tiny changes in the details of the calculations can lead to a different ground state. In particular, if the ground state in  $N = 59$  in Sr were oblate instead of prolate (they are separated by less than 0.5 MeV in the calculations) we will get agreement with the experiment. Similarly, in Zr isotopes, if  $N = 60$  were prolate instead of oblate (separated by 0.2 MeV in the calculations) we would match the experimental jump. In Fig. 3(a) we also recognize a difficulty

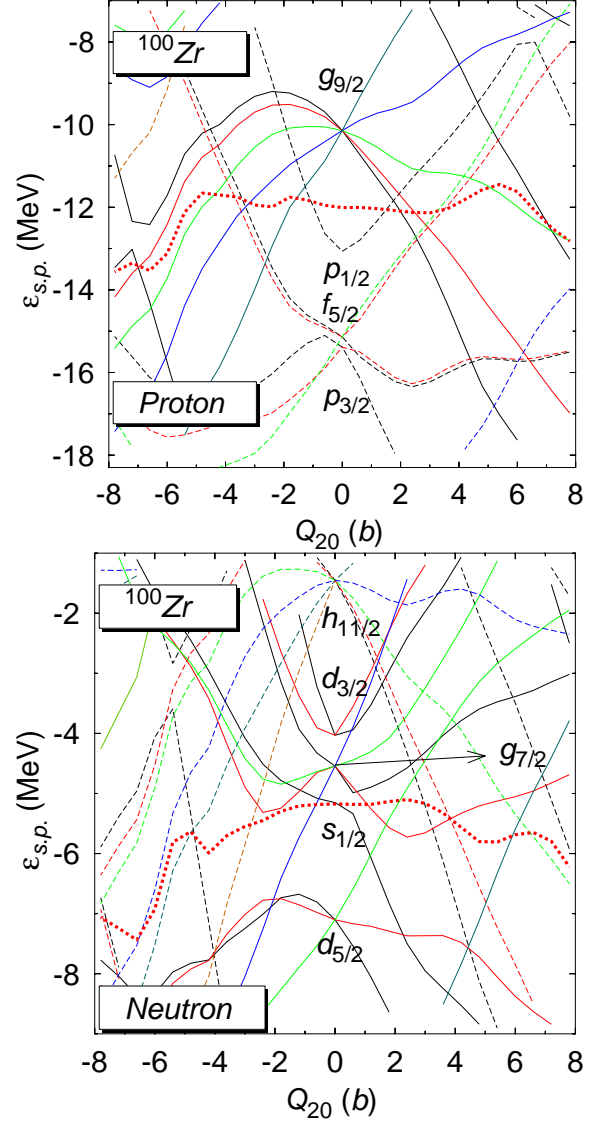


Figure 7: Proton and neutron SPEs for  $^{100}\text{Zr}$  ( $Z = 40, N = 60$ ) as a function of the axial quadrupole moment  $Q_{20}$  (b). The Fermi level is plotted by a thick dotted line.

in the reproduction of the data in the heavier isotopes, since the oblate shapes, which are the ground states, underestimate them. However, we can see that the prolate shapes, which are close in energy, agree with the data. To get a further insight into the reason for this discrepancy and for the fact that the observed jump at  $N = 60$  in Sr and Zr almost vanishes in Mo, we have performed triaxial calculations for the critical isotopes around  $N = 60$ . Similar calculations can also be found in Ref. [18]. We can see in Figs. 4, 5 and 6 the  $Q - \gamma$  plots for  $N = 58, 60$  and  $62$  in Sr (Fig. 4) and Zr (Fig. 5), as well as for  $N = 58, 60, 62, 64, 66$  and  $68$  in Mo isotopes (Fig. 6). In these figures we can see that in Sr and Zr isotopes the transition from oblate to prolate at  $N = 60$  is manifest, suddenly changing from deformations with  $Q \sim 2$  b in the oblate sector to  $Q \sim 5$  b in the prolate one. On the contrary, in Fig. 6 for Mo isotopes we see that the oblate shape at  $N = 58$  becomes gradually triaxial as  $N$  increases. An island of triaxiality is apparent from  $N = 60$  up

to  $N = 68$ . We have calculated the charge radii corresponding to these triaxial configurations that become ground states and have added them in Fig. 3(a) with open squares. The new  $\delta\langle r_c^2 \rangle$  values for these isotopes are now very close to the axial-prolate values and agree very nicely with the experiment. One should notice that one important ingredient for the agreement achieved is that the location of the quadrupole  $Q$ -value for the triaxial minima is much closer to the axial prolate minima than to the oblate ones, which are lower.

To further illustrate the emergence and competition of deformed configurations in this mass region, we show in Fig. 7, for the case of  $^{100}\text{Zr}$  ( $Z = 40$ ,  $N = 60$ ), the proton and neutron single-particle energies (SPE) as functions of the axial quadrupole moment  $Q_{20}$ . Fermi levels are plotted with thick dotted lines. These diagrams help us to identify the regions of low level density, which favor the onset of deformation (Jahn-Teller effect), as well as to stress the important role of the interplay between the proton  $\pi g_{9/2}$  and the neutron  $\nu h_{11/2}$  orbitals (Federman-Pittel effect) to generate deformed configurations [11]. In the plot for the proton SPE we observe an energy gap below the Fermi level at  $Q_{20} = 5$  b, which favors the onset of prolate deformation in Sr isotopes. On the other hand, above the Fermi energy, the low level density on the oblate sector favors oblate configurations in Mo isotopes. In the case of neutrons the energy gap below the Fermi level at  $Q_{20} = -2.5$  b favors oblate shapes in lighter isotopes ( $N < 60$ ), whereas the energy gap above the Fermi level at  $Q_{20} = 5$  b favors prolate shapes in heavier isotopes ( $N > 60$ ). Thus, these simple ideas offer a qualitative understanding of the various mechanisms leading to deformation in this mass region.

#### 4. Conclusions

We have used self-consistent HFB calculations based on the interaction Gogny-D1S to study neutron separation energies and charge radii in neutron-rich Sr, Zr, and Mo isotopic chains. Our primary aim has been to search for signatures of structural changes, and more specifically, for shape transitions in these observables. We have found these correlations and specifically a remarkable connection between shape transitions and sudden changes in the behavior of the isotopic dependence of the nuclear charge radii. The different sensitivities of  $S_{2n}$  and  $\delta\langle r_c^2 \rangle$  can be understood because shape transitions take place in this mass region through isotopes characterized by shape coexistence, where the energies of the various shapes are almost degenerate. Thus, neutron separation energies are not particularly sensitive to these changes. On the other hand, the sensitivity to shape transitions is enhanced for charge radii, specially when the transition takes place suddenly between nuclear shapes at different absolute values of the deformation parameter.

As compared to Sr and Zr isotopes, we have found that Mo isotopes exhibit a smoother increase in the charge radii with the number of neutrons, which is in good agreement with the experimental data. Triaxial degrees of freedom are required to get this agreement beyond  $N = 60$ . From triaxial calculations we have shown that Sr and Zr isotopes suffer a sharp transition from oblate to prolate shapes at  $N = 60$ . On the other hand Mo

isotopes display a smooth transition through a wide region of triaxiality.

In summary, we have shown the ability of the isotopic differences in nuclear charge radii to signal structural changes related to deformation. We have also demonstrated the capability of HFB Gogny-D1S calculations to reproduce those features and therefore to make predictions in unexplored regions.

#### Acknowledgments

This work was supported by MICINN (Spain) under research grants FIS2008-01301, FPA2009-08958, and FIS2009-07277, as well as by Consolider-Ingenio 2010 Programs CPAN CSD2007-00042 and MULTIDARK CSD2009-00064. One of us (R.R.) would like to thank both Prof. J. Äystö and Dr. I. Moore from the University of Jyväskylä for valuable discussions.

- [1] R.F. Casten and B.M. Sherrill, Prog. Part. Nucl. Phys. 45 (2000) S171; M.V. Stoitsov *et al.*, Phys. Rev. C 68 (2003) 054312; D. Vretenar *et al.*, Phys. Rep. 409 (2005) 101; J. Dobaczewski *et al.*, Prog. Part. Nucl. Phys. 59 (2007) 432.
- [2] J.J. Cowan, F.-K. Thielemann and J.W. Truran, Phys. Rep. 208 (1991) 267.
- [3] J. L. Wood *et al.*, Phys. Rep. 215 (1992) 101.
- [4] H. Mach *et al.*, Nucl. Phys. A 523 (1991) 197.
- [5] C. Goodin *et al.*, Nucl. Phys. A 787 (2007) 231c.
- [6] W. Urban *et al.*, Nucl. Phys. A 689 (2001) 605.
- [7] H. Hua *et al.*, Phys. Rev. C 69 (2004) 014317.
- [8] J. Dobaczewski *et al.*, Phys. Rev. C 53 (1996) 2809.
- [9] J. Dechargé and D. Gogny, Phys. Rev. C 21 (1980) 1568.
- [10] J. F. Berger, M. Girod, and D. Gogny, Nucl. Phys. A 428 (1984) 23c.
- [11] L.M. Robledo *et al.*, J. Phys. G 36 (2009) 115104; R. Rodríguez-Guzmán *et al.*, Phys. Rev. C 81 (2010) 024310.
- [12] S. Perez-Martin and L.M. Robledo, Phys. Rev. C 78 (2008) 014304.
- [13] N. Schunck *et al.*, Phys. Rev. C 81 (2010) 024316.
- [14] J.W. Negele, Phys. Rev. C 1 (1970) 1260.
- [15] N. Tajima *et al.*, Nucl. Phys. A 551 (1993) 434.
- [16] P.-G. Reinhard and H. Flocard, Nucl. Phys. A 584 (1995) 467.
- [17] F.C. Charlwood *et al.*, Phys. Lett. B 674 (2009) 23.
- [18] [www-phynu.cea.fr/science\\_en\\_ligne/carte\\_potentiels\\_microscopiques/carte\\_potentiel\\_nucleaire\\_eng.htm](http://www-phynu.cea.fr/science_en_ligne/carte_potentiels_microscopiques/carte_potentiel_nucleaire_eng.htm)
- [19] P. Möller, J. R. Nix, W. D. Myers, and W. J. Swiatecki, At. Data Nucl. Data Tables 59 (1995) 185.
- [20] P. Möller *et al.*, At. Data Nucl. Data Tables 94 (2008) 758.
- [21] J. Skalski, S. Mizutori, and W. Nazarewicz, Nucl. Phys. A 617 (1997) 281.
- [22] F. R. Xu, P. M. Walker, and R. Wyss, Phys. Rev. C 65 (2002) 021303(R).
- [23] G. A. Lalazissis, S. Raman, and P. Ring, At. Data Nucl. Data Tables 71 (1999) 1.
- [24] P. Bonche *et al.*, Nucl. Phys. A 443 (1985) 39.
- [25] M. Bender, G.F. Bertsch, and P.-H. Heenen, Phys. Rev. C 73 (2006) 034322; *ibid.* C 78 (2008) 054312.
- [26] J.-P. Delaroche *et al.*, Phys. Rev. C 81 (2010) 014303.
- [27] U. Hager *et al.*, Phys. Rev. Lett. 96 (2006) 042504.
- [28] F. Buchinger *et al.*, Phys. Rev. C 41 (1990) 2883.
- [29] P. Campbell *et al.*, Phys. Rev. Lett. 89 (2002) 082501.